NANO · MICRO small
www.small-journal.com

Atomic-Scale Mechanism of Spontaneous Polarity Inversion in AlN on Nonpolar Sapphire Substrate Grown by MOCVD

Zhiqiang Liu, Bingyao Liu, Fang Ren, Yue Yin, Shuo Zhang, Meng Liang, Zhipeng Dou, Zhetong Liu, Shenyuan Yang,* Jianchang Yan, Tongbo Wei, Xiaoyan Yi, Chaoxing Wu, Tailiang Guo, Junxi Wang, Yong Zhang,* Jinmin Li, and Peng Gao**

The performance of nitride devices is strongly affected by their polarity. Understanding the polarity determination and evolution mechanism of polar wurtzite nitrides on nonpolar substrates is therefore critically important. This work confirms that the polarity of AlN on sapphire prepared by metal–organic chemical vapor deposition is not inherited from the nitrides/sapphire interface as widely accepted, instead, experiences a spontaneous polarity inversion during the growth. It is found that at the initial growth stage, the interface favors the nitrogen-polarity, rather than the widely accepted metal-polarity or randomly coexisting. However, the polarity subsequently converts into the metal-polar situation, at first locally then expanding into the whole area, driven by the anisotropy of surface energies, which results in universally existing inherent inverse grain boundaries. Furthermore, vertical two-dimensional electron accumulation originating from the lattice symmetry breaking at the inverse grain boundary is first revealed. This work identifies another cause of high-density defects in nitride epilayers, besides lattice mismatch induced dislocations. These findings also offer new insights into atomic structure and determination mechanism of polarity in nitrides, providing clues for its manipulation toward the novel hetero-polarity devices.

1. Introduction

In the absence of inversion symmetry along the c-direction, group III-nitride materials on sapphire substrates (AlN, GaN, InN) and their alloys can exhibit either an N-polar or a metal- (Al, Ga, In) polar surface.[1] Here, N-polar or metal-polar refers to the situation where the epilayer grows along the c or $-c$ direction. Although having identical bulk properties (e.g., refractive index, bandgap, etc.), the two polarities exhibit noticeable differences in surface energy,[2] growth mode,[3] nonlinear optical property,[4] and susceptibility to chemicals.[5] Manipulating the polarity, therefore, is a fertile playground for discovering novel device concepts in form of heteropolar junctions, such as nonlinear optical devices,[3,4,6] polar discontinuity devices,[7] and high-performance GaN high-electron-mobility transistors (HEMT).[8] Particularly, a number of

Z. Q. Liu, F. Ren, Y. Yin, S. Zhang, M. Liang, J. C. Yan, T. B. Wei, X. Y. Yi, J. X. Wang, J. M. Li
Research and Development Center for Semiconductor Lighting Technology
Institute of Semiconductors
Chinese Academy of Sciences
Beijing 100083, China
E-mail: lzq@semi.ac.cn

Z. Q. Liu, F. Ren, Y. Yin, S. Zhang, M. Liang, S. Y. Yang, J. C. Yan, T. B. Wei, X. Y. Yi, J. X. Wang, J. M. Li
Center of Materials Science and Optoelectronics Engineering
University of Chinese Academy of Sciences
Beijing 100049, China

B. Y. Liu, Z. P. Dou, Z. T. Liu, P. Gao
Electron Microscopy Laboratory
and International Center for Quantum Materials
School of Physics
Peking University
Beijing 100871, China
E-mail: p-gao@pku.edu.cn

The ORCID identification number(s) for the author(s) of this article can be found under https://doi.org/10.1002/smll.202200057.

DOI: 10.1002/smll.202200057

B. Y. Liu, Z. P. Dou, Z. T. Liu, P. Gao
Beijing Graphene Institute (BGI)
Beijing 100095, China

B. Y. Liu, Z. T. Liu, P. Gao
Academy for Advanced Interdisciplinary Studies
Peking University
Beijing 100871, China

S. Y. Yang
State Key Laboratory for Superlattices and Microstructures
Institute of Semiconductors
Chinese Academy of Sciences
Beijing 100083, China
E-mail: syyang@semi.ac.cn

C. X. Wu, T. L. Guo
College of Physics and Information Engineering
Fuzhou University
Fuzhou, Fujian 350108, China

Y. Zhang
Department of Electrical and Computer Engineering
The University of North Carolina at Charlotte
Charlotte, NC 28223, USA
E-mail: yong.zhang@uncc.edu

P. Gao
Collaborative Innovation Center of Quantum Matter
Beijing 100871, China

record results of GaN-based HEMT devices have been reported only from the N-polar GaN.[8]

The polarity of the nitride epilayer, intuitively, should be governed by the initial state of the hetero-interface during the epitaxial growth, implying that the nitride epilayer should have a well-defined polarity. However, the exact atomic arrangements of nitrides/sapphire interface and buffer layer remain unclear. The challenges partly arise from the peculiarity of the surface structure of the sapphire substrate. As known, the atomic coordination types for sapphire ($R\bar{3}c$) and nitrides ($P6_3mc$) are completely different. Except for the pseudo-hexagonal oxygen sublattice that possesses a sixfold hexagonal structure, the symmetry of Al_2O_3 is often observed as a threefold triclinic structure.[9] In this case, the (0001) "pseudo-plane" Al^{3+} cations lie on two distinct (0001) planes,[9a] which makes the analysis of the nitrides/sapphire interface extremely complicated. In reality, the polarity of epitaxial nitrides on the nonpolar sapphire surface has been found to exhibit metal-polar,[10] nitrogen-polar,[11] even mixed-polar in some cases,[12] indicating that the heterointerface is not the sole factor in determining the polarity. It has been found the polarity of nitrides may undergo a process of inversion, by introducing foreign atoms during the process of epitaxy away from the nitrides/sapphire interface, such as O-doping,[13] a bi-layer of Al,[10] heavy Mg-doping, or III–V ratio.[14] A number of mechanisms have been speculated accordingly: 1) the pseudobinary Al_2O_3-AlN system,[13] 2) stacking faults.[10] Unfortunately, most of the previous conclusions are speculative based on the characterization (e.g., wet etching[15] or convergent beam electron diffraction[16]) of the epilayer near the surface, however, far away from the substrate–epilayer interface. Therefore, atomic evidence and the polarity evolution process are largely absent. Liu et al. attempted to explain the polarity evolution by providing direct experimental evidence of scanning transmission electron microscopy (STEM). However, the *Z*-contrast STEM image there was too blurry to identify the polarity at the sapphire/AlN interface.[16a] Furthermore, the information on the initial stage of growth and the microscopic scale structural information of the inversion is largely lacking. To unambiguously understand the underlying mechanism that causes the polarity inversion and that determines the polarity of the epilayer, logically, a few basic questions should be answered: 1) What is the initial polarity of the growth starting from the substrate, nitrogen-polar, metal-polar, or randomly mixed of the two? 2) What is the role of the atomistic structure of the substrate? 3) Will the polarity inversion still exist if no doping is involved? 4) How and why is an IDB formed? Unambiguous answers to these questions will lead to the answers to the ultimate questions: why do the nitride epilayers prepared by metal–organic chemical vapor deposition (MOCVD) mostly end up in the highly identical metal-polar?[5a] and how to, at least in principle, control the polarity of nitrides? This work explicitly addresses these questions for the first time.

P. Gao
Interdisciplinary Institute of Light-Element Quantum Materials and Research Center for Light-Element Advanced Materials
Peking University
Beijing 100871, China

In this work, the atomic structure and the growth process of the nitride buffer layer are revealed at the atomic scale. We observe that at the initial growth stage, the heterointerface favors the nitrogen-polarity, which is contradicted to the widely accepted metal-polarity. However, during the subsequent growth, because of the variation in the step height of the sapphire substrate (originating from the (0001) "pseudo-plane" Al^{3+} cations), lateral Inversion Domain Boundaries (IDBs) form when the domains coalesce. Thereafter, because of the growth rate disparity of the two phases, the metal-polar gradually dominates over the nitrogen-polar, at first locally then expanding into the whole area. Therefore, polarity switching is a spontaneous process without the need of incorporating any foreign atoms. The atomic structure of lattice inversion boundary is identified by atomic-scale direct observation and theoretical calculation, i.e., the polarity inversion happens at (10–10) r-face through a boundary with eightfold and fourfold coordinated bonds, not the commonly expected (0001) c-face. Furthermore, the driving force of such a polarity inversion is also clarified. These findings advance the current understanding of polarity determination and also lay the theoretical foundation for designing novel hetero-polarity devices.

2. Results and Discussion

2.1. Characterization of the Polarity of AlN Epilayer

To clarify the process of polarity selection, an AlN layer was grown on the nitridated sapphire substrate using an AlN buffer layer method. The atomically resolved STEM high angle annular dark-field (HAADF) images of the nitrides either at or far from the nitride/sapphire interface with a view direction of [11–20] reveal the totally different polarities: N-polar at the heterointerface (**Figure 1**a), but Al-polarity near the top surface of the nitride film (Figure 1b). The polarity preserves till as far as the surface of the epitaxy layer, as confirmed by the V-pits morphology after wet-etching (Figure 1c).[17] Therefore, it is reasonable to speculate that stacking faults and/or inverse domain boundaries are generated during the process of the nitride growth.

2.2. The Atomic-Scale Growth Processes at the Nitride/Sapphire Interface

Firstly, the possible initial growth states, i.e., sapphire nitridation and AlN buffer layer deposition, are simulated by density functional theory (DFT) calculations. Typically, the epitaxial layer inherits the crystallinity from the substrate. However, it is not the case for the nitrides grown on sapphire. The stacking order of sapphire along the pseudohexagonal c-axis is R-$AlAlO_3$-$AlAlO_3$-R, where R represents the continuing sequence in the bulk. The most stable surface is a single Al layer termination that has the same stoichiometry as the bulk,[18] as shown in **Figure 2**a, in which the low-site Al and high-site Al are exhibited.[9a] Four possible interfacial configurations are shown in Figure 2b–e. We find that nitrogen-polar configuration-1 (Figure 2b) with an adsorption energy of ≈−3.8 eV is the most

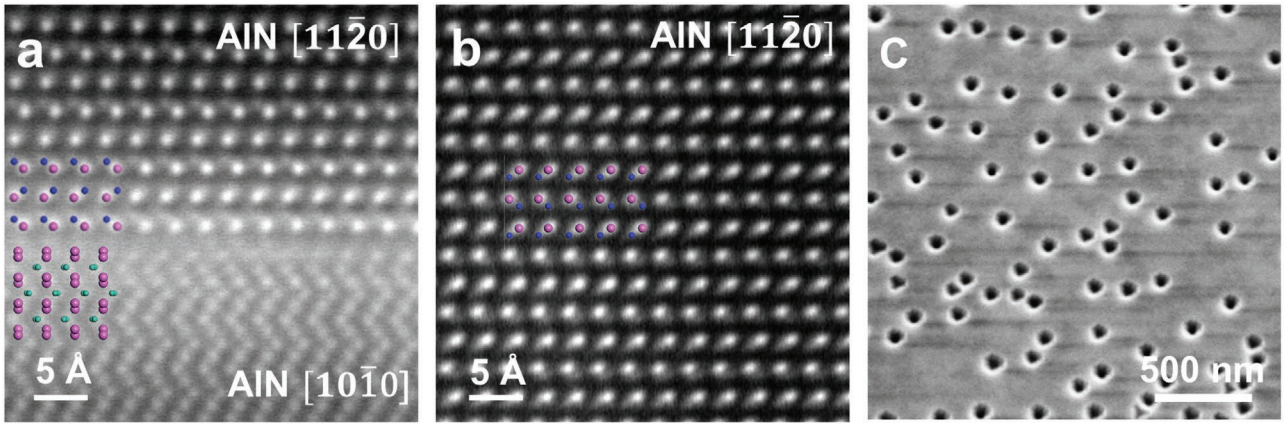

Figure 1. Characterization of the polarity of AlN epi-layer: a) A cross-sectional HAADF image taken at the AlN/sapphire interface along the AlN[11–20] direction. The nitrides lattice exhibits N-polar. b) A cross-sectional HAADF image taken near the top surface of the AlN epilayer along the AlN [11–20] direction, where the stacking order of the nitrides has converted into Al-polar. The violet, blue, and cyan balls represent Al, N, and O atoms, respectively. c) Surface morphology of KOH etched AlN surface. The hexagonal V-pits indicate metal polarity.

stable configuration (Table S1, Supporting Information), which corresponds to the process of sapphire nitridation, and the following cation Al layer bonding with such adsorped N atoms (**Figure 3**g–h) will serve as the interfacial layer for the further epitaxial growth of AlN.

The X-ray photoelectron spectroscopy (XPS) spectra of the nitridated sapphire (Figure 2f–g), further support the above conclusion. The spectra exhibit distinct N^{1s} and Al^{2p} core-level photoelectron peaks, indicating that nitrogen is bonded to the sapphire surface and the Al–N bonds are formed.

2.3. Characterization of the AlN/Sapphire Interface

The atomically resolved HAADF image of the nitride/sapphire interface with a view direction of AlN [10–10] is shown in Figure 3a. The lattice-misfit, as expected, is observed by the Inversed Fast Fourier Transform (IFFT) algorithm image (Figure 3b), which is obtained from the in-plane Bragg reflections as shown in the pair of blue circles in the inset of Figure 3b. There are a few interesting features. First, the high-Al sites are occupied by an additional layer of Al atoms

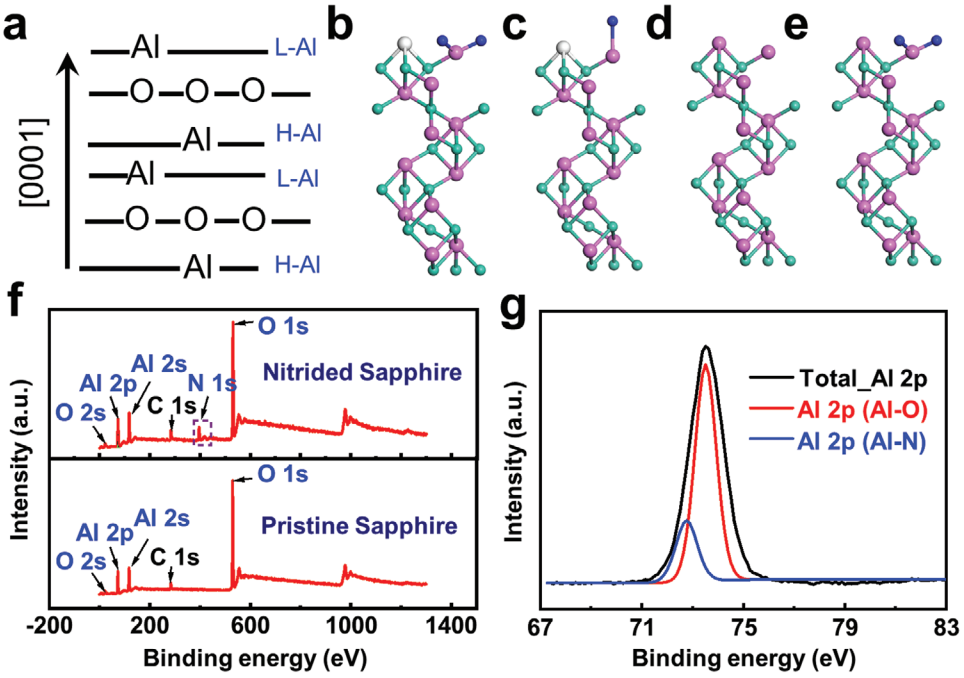

Figure 2. First-principles calculations of the abortion of incoming atoms on the sapphire surface: a) The atomic arrangement and stacking order of sapphire. b) Configuration-1, nitrogen atoms bonded to the low-Al with a nitrogen polar ordering. c) Configuration-2, nitrogen atoms bonded to the low-Al with an aluminum polar ordering. d) Aluminum atoms bonded to the high-Al site. e) Nitrogen atoms bonded to the low-Al after the high-Al occupation. Cyan ball: oxygen. Violet ball: aluminum. Blue ball: nitrogen. White ball: vacancy of Al. f) C1s XPS spectra of the sapphire surface before and after the nitridation process. g) The spectra of Al 2p peak showing the formation of the Al-N bond.

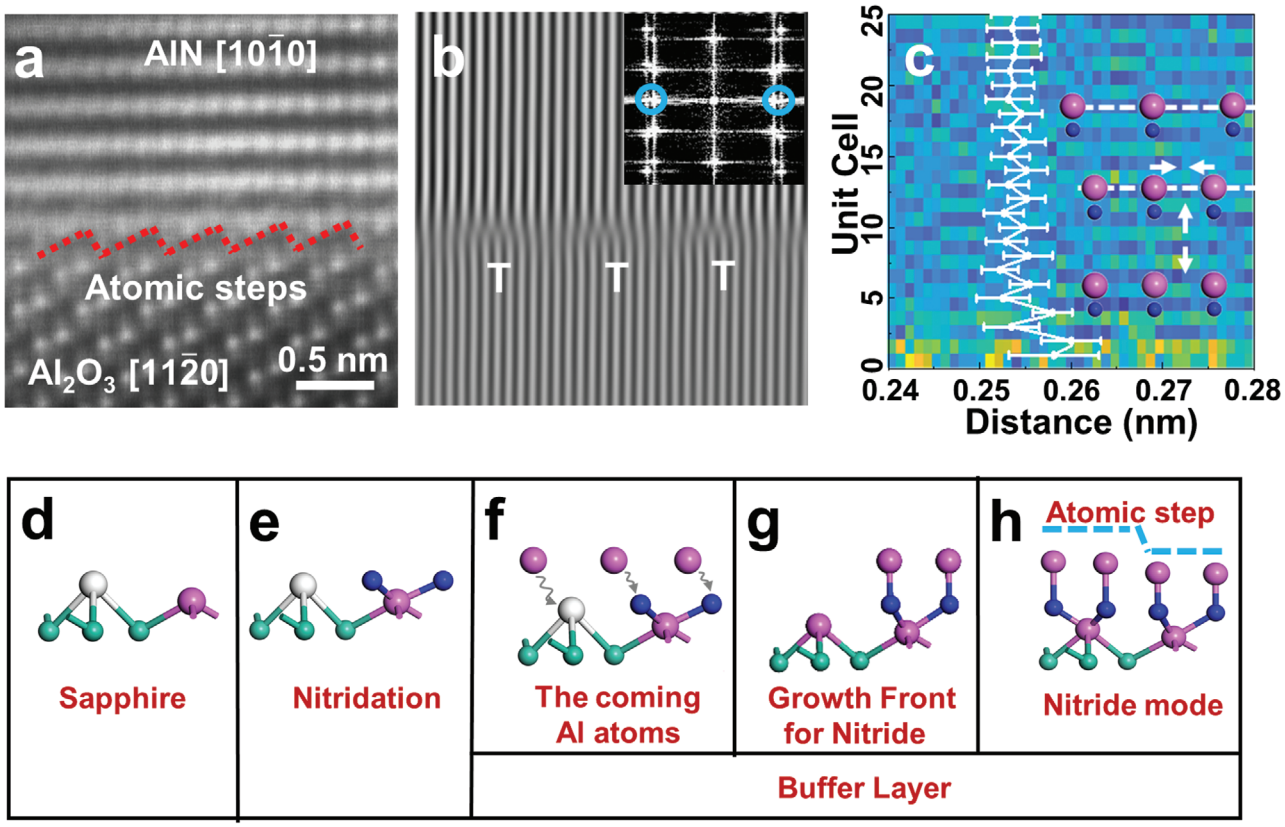

Figure 3. Atomic structure of the AlN/sapphire interface: a) A cross-sectional HAADF image taken at the interface of the AlN/sapphire interface along AlN [10–10] direction. Atomic steps and a periodic zigzag structure are seen at the interface, showing the misfit dislocation arrays. b) IFFT image of the interface between nitrides and sapphire. The inset pattern in (b) is obtained via Fast Fourier Transform of (a). c) The d-spacing of the c-planes of the AlN layer adjacent to the interface based on quantitative measurements. The first Al-N layer exhibits the biggest d-spacing of c planes due to the lattice mismatch and peculiar atomic coordination of Al atoms in sapphire, which results in the shrinking of the in-plane lattice. The atomic-scale growth processes at the nitride/sapphire interface: d) The atomic configuration of a primitive sapphire surface, in which the low-Al sites are occupied. e) Binding of the arriving nitrogen atoms to the low-site Al, corresponding to the process of sapphire nitridation. f) The occupation of the high-Al sites. g) The formation of the growth front for the nitride at the AlN/sapphire interface. h) The growth evolves to the normal nitride mode gradually. Cyan ball: oxygen. Violet ball: aluminum. Blue ball: nitrogen. White ball: vacancy of Al. The atomic models are observed along [1–210] of sapphire.

(Figure S1, Supporting Information). Second, we observe atomic steps at the interface (Figure 3a), which exhibit a periodical zigzag feature, resulting in a bigger average d-spacing of *c*-planes (Figure 3c). After only—two to three monolayers, it nearly relaxes to the standard bulk AlN structure and such zigzag feature vanishes. We suggest that the periodical zigzag is originated from the pseudohexagonal lattice of sapphire, in which Al atoms lie in different *c*-planes (Figures 2a and 3a). The formation mechanism of such special structure will be investigated by DFT calculations below.

Based on the above-mentioned experimental observation, Figure 3d–h shows the step-by-step growth process of the nitride buffer layer from the DFT simulations. First, starting from the sapphire substrate (Figure 3d), the arriving nitrogen atoms bind to the low-site Al, corresponding to the process of sapphire nitridation (Figure 3e) in the typical nitrogen-rich condition. Subsequently, the role of low temperature is to create a metal-rich condition corresponding to the process of forming the buffer layer. It promotes the binding of incoming Al atoms simultaneously to the top surface oxygen and nitrogen atoms (Figure 3f–g), even though they have different adsorption energies (Table S2, Supporting Information). This model is consistent with the STEM image (Figure S1, Supporting Information). Otherwise, incomplete coverage of the Al atomic layer will introduce additional stress and defects. Then, the atomic stacking continues in the sequence of the standard N-polar nitride structure (Figure 3f), which is also confirmed by HAADF images of nitrides/sapphire interface (Figure 1a).

As shown in Figure 3h, the first interfacial Al layer of AlN is not perfectly planar or atomically flat but exhibits a step-like feature. The special zigzag atomic arrangement enlarges the average d-spacing of c-planes at the interface, which results in the shrinking of the in-plane lattice and provides an additional factor to accommodate the interfacial mismatch. In addition, the first few Al-N monolayers at the interface also act as a crystal structure transition region, specifically a transition from a triclinic system to a hexagonal one, after which the zigzag structure vanishes. Furthermore, such step-like feature also acts as the driving force for polarity inversion, which will be discussed in the following section.

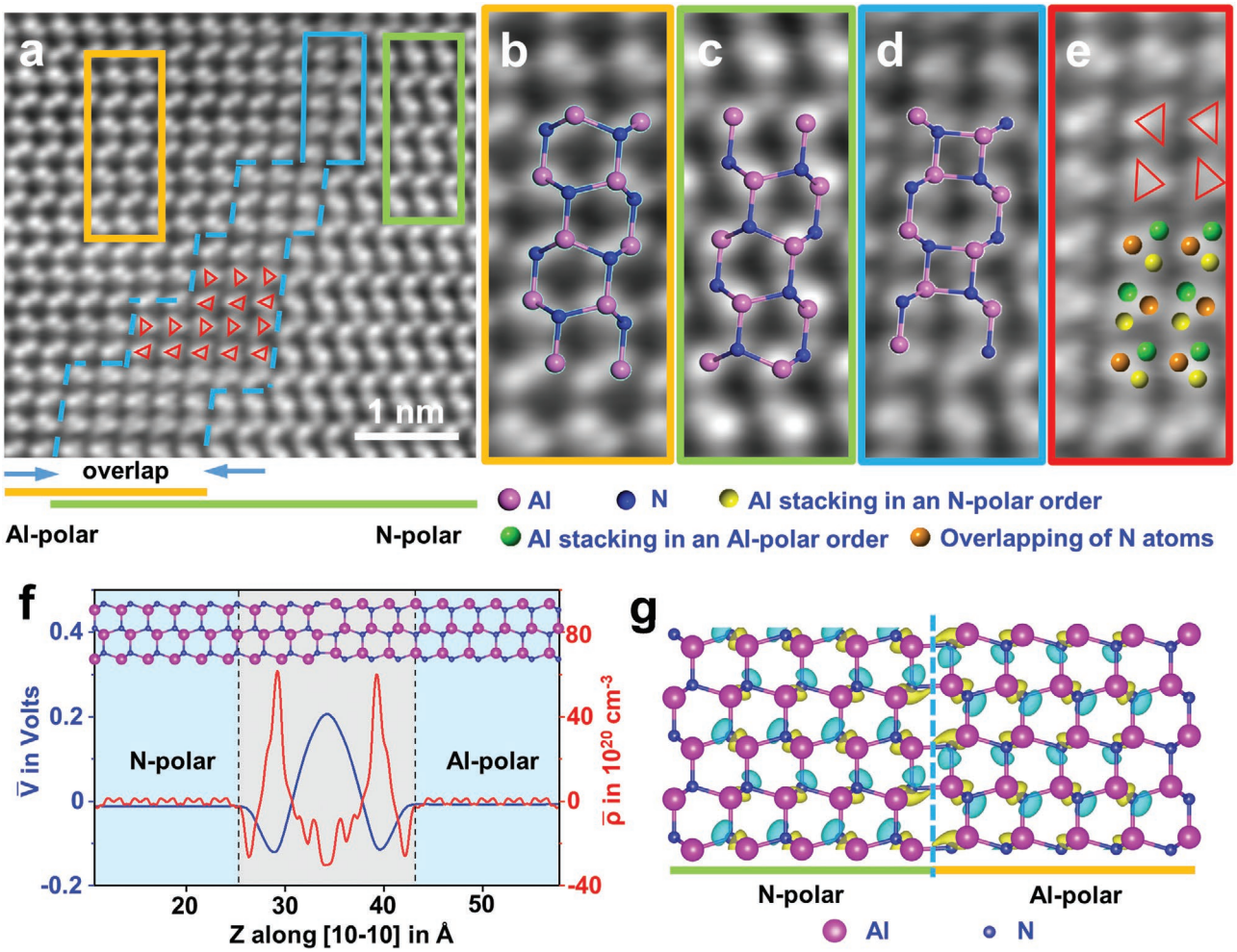

Figure 4. The cross-sectional STEM images of AlN alone AlN [11–20] direction and the atomic arrangements for IDBs: a) Atom-resolved-iDPC image taken at the lattice inversion area, showing that the lattice inversion occurs at (10–10) with a step-like morphology. b) Al-polar and c) N-polar AlN lattice on different sides of the inverse domain boundary, the corresponding ball and stick model is superimposed on the image. d) The detailed structure of the upper part of the inverse domain boundary is shown by superimposing atomic models on the iDPC image. The eightfold and fourfold coordinated bonds appear at the boundary. The atomic coordinate is coincident with that of IDB-1. e) The detailed structure of the lower part of the inverse domain boundary, indicating the overlap of Al-polar and N-polar regions. The green and yellow balls represent the Al atoms in adjacent (11–20) face, which lies in the different side of an inverse domain boundary. f) Plane-averaged electrostatic potential profile (blue) $V(z)$ and total charge density (red) $\rho(z)$ along the [10–10] direction in IDB. g) Differential charge density at the IDB. Yellow color indicates electron accumulation and cyan color indicates electron depletion. An obvious electron depletion can be observed at the polar inversion interface. Therefore, the net the positive sheet charge is produced. It is consisted with the result of total charge density (red) $\rho(z)$ in f).

2.4. Characterization and Identification of Inversion Domain Boundary

As illustrated above, the initial state of nitride growth leads to a N-polar nitride epilayer. However, most of the nitride layers grown by MOCVD finally exhibit metal-polarity, which implies that a polarity change associated withthe formation of inversion domain boundary (IDB) happens during the growth. Integrated Differential Phase Contrast (iDPC) can show the light atoms better when they coexist with other heavier atoms, therefore we use iDPC to depict the interface bonding functions and the structure of the polarity inversion boundary. As shown in **Figure 4**a–c, indicated by a clearly observed inverse domain boundary in (10–10) face (between the blue dash lines in Figure 4a), the polarity inversion occurs gradually at (10–10) face, as opposed to the commonly believed (0001) face.[13]

Based on the STEM observations, two types of atomic models defined as IDB-1 and IDB-2 are considered as shown in Figure S2a,b (Supporting Information).[19] Another two natural choices associated with polarity inversion are stacking faults in the (0001) *c*-plane, which are referred to as bi-layer nitrogen or metal (Al) monolayer. We denote them as IDB-3 and IDB-4 (Figure S2c,d, Supporting Information). We find IDB-1 with formation energy –0.24 eV Å^{-2} is the most stable configuration (Table S3, Supporting Information). The reason for this lies in the fact that IDB-2, which can be obtained by translating one side of IDB-1 along the *c*-axis by *c*/2, contains both Al–Al and N–N bonds at the boundary. Such wrong bonds increase the

total energy and thereby reduce the stability of the system. As shown in Figure 4d, the appearance of the eightfold and fourfold coordinated bonds at the boundary provides direct evidence that the polarity inversion is realized via IDB-1. Furthermore, a series of peculiar triangle patterns are clearly shown at the lower part of the boundary (Figure 4e), which are attributed to the overlap of nitrogen atoms from different sides of IDB-1, i.e., N-polar and Al-polar regions and results in a defective transition region. This observation again proves our model based on the theoretical and experimental results. The identification of IDB-1 is further confirmed by the breaking of translation symmetry of hexagonal lattice at the domain boundary. As shown in Figure S2a (Supporting Information), IDB-1 induces a mirror-like image domain at the boundary, which agrees with the experimental results (Figure 4b,c). While on the contrary, IDB-2 keeps the translation-like symmetry across the domain boundary.

The atomic arrangements of IDB-3 and IDB-4 are similar to that of IDB-2, thereby not energetically favorable. Another possible configuration (IDB-5) is also considered and proven to be unstable (Figure S2e, Supporting Information). This means that such configuration is only plausible when considering the participation of foreign atoms such as oxygen, which has been demonstrated previously.[13,20] It is interesting to note that one more possible configuration IDB-6 leads to the metal-to-nitrogen polarity inversion (Figure S2f, Supporting Information). And the formation of energy is ≈–0.22 eV Å^{-2}. The difference between IDB-5 and IDB-6 can be understood from the perspective of orbital hybridization. As known, besides typical sp^3 hybridization (tetrahedron),[21] Al atoms can also exhibit sp^3d^2-like hybridization (octahedral), as in the case of Al_2O_3,[22] in which each Al atom bonds to six O atoms.[23] Therefore, as Al atoms serving an interlayer (IDB-6), they can bond with six N atoms lying on both sides of the boundary and form a stable configuration. It can also explain during the process of sapphire nitridation, why the incoming N atoms prefer forming 3N-Al unit with configuration-1 (Figure 2b, N-polar), instead of N-Al unit with Configuration-2 (Figure 2c, Ga-polar). In summary, without the participation of foreign atoms, IDB-1 is the energetically most favorable one.

Since the IDB-1 structure is located on the (10–10) plane, it is instructive to compare the formation energy of the boundary with that of the (10–10) plane in bulk nitrides. Not surprisingly, we find lattice inversion is an energy-gaining process (Table S3, Supporting Information). In this case, however, another factor should also be considered. Based on the previous calculation results, the (0001) face of nitrides is about 0.2 eV Å^{-2} lower in energy than (000–1) surface in the metal-rich atmosphere,[2] which is typical for MOCVD. Therefore, the energy cost of forming IDB can be compensated by the polarity exchange of the growth front and the formation of IDB turns out to be energetically favorable.

Another driving force for the polarity inversion is coming from the (0001) "pseudo-plane" of sapphire substrates with both high-site and low-site of Al^{3+} cations. The lattice of the following nitride nuclei gets the atomic registry from the substrate and exhibits N-polarity, however, different heights (Figure 3a,h). When the isolated islands meet during the subsequent coalesce process, bonds will be misaligned, thus, resulting in the IDB, specifically IDB-1 with the lowest formation energy on the (10–10) plane.

Together with Figure 1a, the polarity selection and evolution process can be described as follows: The nitride grown on sapphire tends to be N-polar initially determined by the atomic configuration of the sapphire surface shown in Figure 1a. However, N polarity cannot be maintained under the standard MOCVD growth condition. Considering the typical layer by layer growth mode, the nitride epilayer subsequently transfers to metal-polar with lower surface energy in some local areas by the formation of a low-energy IDB at the (10–10) plane (Figure S3a–c, Supporting Information). Therefore, the polarity inversion occurs horizontally, not vertically. Now, with the readily formed mixed polarity growth front, the (000–1) facet with a slower growth rate will be covered gradually due to the passivation of hydrogen atoms, and difference in surface energy.[24] As shown in Figure S3a–c (Supporting Information), the N-polar area grows narrower as the thickness increases and vanishes at around 100 nm away from the sapphire substrate. Figure S3d–g (Supporting Information) shows the atomic resolution HAADF images at selected locations (labeled with blue numbers) on the polarity IDBs in Figure S3b (Supporting Information), from which we can clearly see the inversion process.

Electron energy loss spectra (EELS) across the polarity inversion area clearly show no oxygen accumulation at the inversion boundary, which rules out the possibility of oxygen participation in the lattice inversion process in our sample (Figure S4, Supporting Information).

The plane-averaged electrostatic potential profile and the average charge are computed in a supercell containing an IDB-1 (Figure 4f). Integration of the charge density around the boundary gives a net sheet charge of 1.9×10^{12} cm^{-2}, which is comparable with that at the interface of $Al_{0.15}Ga_{0.85}N$/GaN heterojunction.[25] To understand the formation mechanism, the differential charge density and charge transfer calculations at the polar-inversion interface is performed. As shown in Figure 4g, the breaking of lattice symmetry at the Al-polar/N-polar interface leads to the redistribution of valence electrons.[6e] As a result, an obvious electron depletion can be observed, and a positive sheet charge is formed. Free electrons will tend to compensate for the polarity-inversion induced sheet charge at the abrupt polarity-inversion interface (Figure 4a), resulting in the accumulation of two-dimensional (2D) electrons. With this understanding, we emphasize that the formation mechanism of the electron accumulation in the current system is distinctly different from that in GaAs/AlGaAs (modulation doping)[26] or GaN/AlGaN (polarization effect) heterojunction.[25] It provides an interesting possibility for novel device applications with a vertical 2D conductive channel. In the meantime, it may also act as a leakage channel or shunt and deteriorate the breakdown performance of high-power (Schottky diodes) and high frequency (HEMT) nitride devices.[27]

We would like to point out that the stacking order of nitrides is affected by many factors, including V/III ratio, temperature, and nitridation process, besides the atomic configuration of the interface and MOCVD atmosphere. For example, the participation of foreign species, such as oxygen incorporation[13,20b] and substantial nitrogen in sapphire,[28] may result in an intricate

system thus affecting the polarity in a more complicated manner, which requires further systematic study to clarify their effects on the polarity control.

3. Conclusion

To conclude, the mechanism of polarity selection and evolution in group-III nitrides on a nonpolar sapphire substrate is first established. We have shown that the nitrides grown on sapphire tend to be N-polar initially, which is contrary to the common belief of metal-polarity at the initial state. It subsequently transfers to metal-polar in local areas by the formation of a low-energy IDB at the (10–10) plane. Further growth eventually leads to the full conversion to the metal-polar. It is an inherent and spontaneous process and does not need the participation of foreign atoms. We find, besides lattice mismatch, the universal existence of IDBs should be another cause of high-density defects in nitride epilayers on nonpolar sapphire substrates prepared by MOCVD. The symmetry of sapphire substrate and typical metal-rich condition of MOCVD, which favors the growth of metal-polarity, plays a crucial role in this process. Based on direct observations and theoretical calculations, the atomic structure leading to the polarity inversion from nitrogen-polarity to metal-polarity is first identified. Furthermore, a novel vertical 2D electron accumulation is revealed at the polarity inversion interface. We point out that such 2D electron accumulation comes from the breaking of lattice symmetry at the polar inversion interface, which is distinctly different from the well-known two-dimensional electron gas systems. All these findings provide valuable insights into the kinetic process and atomic arrangement at the nitrides/sapphire heterointerface. More importantly, it points to a direction for polarity manipulation and heteropolarity device design.

4. Experimental Section

MOCVD Growth: The epitaxy of AlN film was grown by a homemade MOCVD system. During the growth process of nitride films, trimethylaluminum (TMAl) and ammonia (NH_3) were adopted as Al and N precursors. Hydrogen (H_2) acted as the carrier gas during the growth process. A typical two-step method was adopted for AlN growth. First, sapphire was nitridated by NH_3 flow of 4 slm at 1200 °C for 5 min. Then, a thin AlN buffer layer was deposited onto the nitridated surface at a relatively low temperature, with a III–V ratio of 10220 (650 °C). After a high-temperature annealing process, an AlN layer was grown at 1200 °C for 1 h, with a III–V ratio of 5000. The entire epilayer was not intentionally doped. The thickness of AlN layer is 1.2 µm, with a 10 nm buffer layer.

Characterization: The as-grown epitaxial layer was characterized by XPS (PHI VersaProbe III; operated at 4.4 kV). To obtain the atomic resolution image, aberration-corrected STEM with iDPC and HAADF mode (Titan Cubed Themis G2 300, USA, operated at 300 kV) were used. The STEM convergence semi-angle was 30 mrad and the collection semi-angles were 39–200 mrad for HAADF mode and 4–21 mrad for iDPC mode. It should be noted that the iDPC images had an advantage for characterizing light atoms (such as N and O atoms in our case). The atom positions were depicted using a double Gaussion method,[29] as shown in Figure S5 (Supporting Information). The STEM sample was prepared by a focused ion beam (FIB) system, mechanical polishing, and Precision Ion Polishing System (Model 691, Gatan Inc., operated at 3.5 kV). The atomistic models were generated by VESTA.

First-Principles Calculations: The first-principles calculations within DFT were performed using the Vienna Ab initio Simulation Package (VASP). The projector augmented wave pseudopotential and the generalized gradient approximation of Perdew–Burke–Ernzerhof (PBE) were adopted for the exchange-correlation function. The cutoff energy was chosen to be 350 eV and full structural optimization was performed until atomic forces were <0.02 eV $Å^{-1}$.

The adsorption of Al and N adatoms on sapphire was modeled using one adatom in a $1 \times 1 \times 1$ Al_2O_3 supercell (18 O atoms and 12 Al atoms). The adsorption energy is defined as $\Delta E = -(E_{ag} - \mu_a - E_g)$, where E_{ag} is the total energy adatom and the substrate, E_g is the total energy of the isolated sapphire substrate, and μ_a is the chemical potential of Al or N atom.

The polarity inversion was modeled by a supercell with a domain boundary. IBD-1 was constructed with fourfold and eightfold rings of bonds at the boundary. IBD-2 was built by translating one side of an IDB-1 by $c/2$ along the [0001] direction. As illustrated in Figure 4e, in IBD-2 the Ga and N atoms were interchanged as one crossed the (10–10) plane, which resulted in the polarity inversion. IDB-3 was a bi-nitrogen stacking fault lying on AlN (0001) plane, and IDB-4 was a bi-aluminum stacking fault. IDB-5 and IDB-6 were formed by Ga-N bonds, in which nitrogen or aluminum monolayer acted as the interlayer.

To compute the electrical properties of the Al-polar/N-polar interface and reveal the formation mechanism of 2D electron accumulation, we constructed a structure with a $1 \times 2 \times 12$ Al-polar supercell and a $1 \times 2 \times 12$ N-polar supercell, stacking alone [10–10] direction. The domain boundary was constructed with IBD-1. The average electric field inside the structure $\left(\bar{E}(z) = -\frac{\partial \bar{V}(z)}{\partial z}\right)$, the average charge $\left(\bar{\rho}(z) = -\frac{\varepsilon \partial^2 \bar{V}(z)}{\partial z^2}\right)$ were computed from the total electrostatic potential of the structure.

Supporting Information

Supporting Information is available from the Wiley Online Library or from the author.

Acknowledgements

This research was funded by the National Key Research and Development Program of China (Grant numbers, 2019YFA0708202 and 2021YFB3600401), and the National Natural Science Foundation of China (Grant numbers, 61974140, 61604140, 11974023 and 52021006). Y.Z. acknowledges the support of Bissell Distinguished Professorship endowment fund at UNCC.

Conflict of Interest

The authors declare no conflict of interest.

Data Availability Statement

The data that support the findings of this study are available from the corresponding author upon reasonable request.

Keywords

break-down votage, interfaces, metal–organic chemical vapor deposition (MOCVD), nitrides, polarity

Received: January 4, 2022
Revised: January 29, 2022
Published online:

[1] a) T. Hashimoto, F. Wu, J. S. Speck, S. Nakamura, *Nat. Mater.* **2007**, *6*, 568; b) Y. J. Lu, J. Kim, H. Y. Chen, C. H. Wu, N. Dabidian, C. E. Sanders, C. Y. Wang, M. Y. Lu, B. H. Li, X. G. Qiu, W. H. Chang, L. J. Chen, G. Shvets, C. K. Shih, S. Gwo, *Science* **2012**, *337*, 450; c) S. Nakamura, *Science* **1998**, *281*, 956; d) P. Wang, Y. Yuan, C. Zhao, X. Wang, X. Zheng, X. Rong, T. Wang, B. Sheng, Q. Wang, Y. Zhang, L. Bian, X. Yang, F. Xu, Z. Qin, X. Li, X. Zhang, B. Shen, *Nano Lett.* **2016**, *16*, 1328; e) F. Schuster, F. Furtmayr, R. Zamani, C. Magen, J. R. Morante, J. Arbiol, J. A. Garrido, M. Stutzmann, *Nano Lett.* **2012**, *12*, 2199; f) D. Huang, M. A. Reshchikov, P. Visconti, F. Yun, A. A. Baski, T. King, H. Morkoc, J. Jasinski, Z. Liliental-Weber, C. W. Litton, *J. Vac. Sci. Techno. B* **2002**, *20*, 2256.

[2] C. E. Dreyer, A. Janotti, C. G. Van de Walle, *Phys. Rev. B* **2014**, *89*, 081305.

[3] H. Yagi, N. Osumi, Y. Inoue, T. Nakano, *Phys. Status Solidi B* **2018**, *255*, 1700475.

[4] A. Chowdhury, H. M. Ng, M. Bhardwaj, N. G. Weimann, *Appl. Phys. Lett.* **2003**, *83*, 1077.

[5] a) J. Zuniga-Perez, V. Consonni, L. Lymperakis, X. Kong, A. Trampert, S. Fernandez-Garrido, O. Brandt, H. Renevier, S. Keller, K. Hestroffer, M. R. Wagner, J. S. Reparaz, F. Akyol, S. Rajan, S. Rennesson, T. Palacios, G. Feuillet, *Appl. Phys. Rev.* **2016**, *3*, 041303; b) N. A. Sanford, A. V. Davydov, D. V. Tsvetkov, A. V. Dmitriev, S. Keller, U. K. Mishra, S. P. DenBaars, S. S. Park, J. Y. Han, R. J. Molnar, *J. Appl. Phys.* **2005**, *97*, 053512.

[6] a) D. Passeri, M. C. Larciprete, A. Belardini, S. Paoloni, A. Passaseo, C. Sibilia, F. Michelotti, *Appl. Phys. B: Lasers Opt.* **2004**, *79*, 611; b) R. Kirste, S. Mita, L. Hussey, M. P. Hoffmann, W. Guo, I. Bryan, Z. Bryan, J. Tweedie, J. Xie, M. Gerhold, R. Collazo, Z. Sitar, *Appl. Phys. Lett.* **2013**, *102*, 181913; c) J. K. Hite, N. D. Bassim, M. E. Twigg, M. A. Mastro, F. J. Kub, C. R. Eddy Jr., *J. Cryst. Growth* **2011**, *332*, 43; d) R. Katayama, Y. Kuge, T. Kondo, K. Onabe, *J. Cryst. Growth* **2007**, *301–302*, 447; e) M. de la Mata, R. R. Zamani, S. Marti-Sanchez, M. Eickhoff, Q. Xiong, I. M. A. Fontcuberta, P. Caroff, J. Arbiol, *Nano Lett.* **2019**, *19*, 3396.

[7] M. Gibertini, G. Pizzi, N. Marzari, *Nat. Commun.* **2014**, *5*, 5157.

[8] a) S. Rajan, A. Chini, M. H. Wong, J. S. Speck, U. K. Mishra, *J. Appl. Phys.* **2007**, *102*, 044501; b) O. S. Koksaldi, J. Haller, H. Li, B. Romanczyk, M. Guidry, S. Wienecke, S. Keller, U. K. Mishra, *IEEE Electron Device Lett.* **2018**, *39*, 1014; c) S. Wienecke, B. Romanczyk, M. Guidry, H. Li, E. Ahmadi, K. Hestroffer, X. Zheng, S. Keller, U. K. Mishra, *IEEE Electron Device Lett.* **2017**, *38*, 359.

[9] a) P. J. Eng, T. P. Trainor, G. E. Brown, G. A. Waychunas, M. Newville, S. R. Sutton, M. L. Rivers, *Science* **2000**, *288*, 1029; b) J. Ahn, J. W. Rabalais, *Surf. Sci.* **1997**, *388*, 121; c) X. G. Wang, A. Chaka, M. Scheffler, *Phys. Rev. Lett.* **2000**, *84*, 3650.

[10] A. Yoshikawa, K. Xu, *Thin Solid Films* **2002**, *412*, 38.

[11] a) F. Liu, Z. Zhang, X. Rong, Y. Yu, T. Wang, B. Sheng, J. Wei, S. Zhou, X. Yang, F. Xu, Z. Qin, Y. Zhang, K. Liu, B. Shen, X. Wang, *Adv. Funct. Mater.* **2020**, 2001283, https://doi.org/10.1002/adfm.202001283; b) D. Huang, M. A. Reshchikov, P. Visconti, F. Yun, A. A. Baski, T. King, H. Morkoç, J. Jasinski, Z. Liliental-Weber, C. W. Litton, *J. Vac. Sci. Technol. B: Microelectron. Nanometer Struct.* **2002**, 20.

[12] a) R. Dimitrov, M. Murphy, J. Smart, W. Schaff, J. R. Shealy, L. F. Eastman, O. Ambacher, M. Stutzmann, *J. Appl. Phys.* **2000**, *87*, 3375; b) G. Namkoong, W. A. Doolittle, A. S. Brown, M. Losurdo, M. M. Giangregorio, G. Bruno, *J. Cryst. Growth* **2003**, *252*, 159.

[13] S. Mohn, N. Stolyarchuk, T. Markurt, R. Kirste, M. P. Hoffmann, R. Collazo, A. Courville, R. Di Felice, Z. Sitar, P. Vennéguès, M. Albrecht, *Phys. Rev. Appl.* **2016**, *5*, 054004.

[14] a) V. Ramachandran, R. M. Feenstra, W. L. Sarney, L. Salamanca-Riba, J. E. Northrup, L. T. Romano, D. W. Greve, *Appl. Phys. Lett.* **1999**, *75*, 808; b) J. E. Northrup, *Appl. Phys. Lett.* **2003**, *82*, 2278; c) S. Pezzagna, P. Vennegues, N. Grandjean, J. Massies, *J. Cryst. Growth* **2004**, *269*, 249; d) P. Vennéguès, M. Leroux, S. Dalmasso, M. Benaissa, P. De Mierry, P. Lorenzini, B. Damilano, B. Beaumont, J. Massies, P. Gibart, *Phys. Rev. B* **2003**, *68*, 235214; e) W. Luo, L. Li, Z. Li, Q. Yang, D. Zhang, X. Dong, D. Peng, L. Pan, C. Li, B. Liu, R. Zhong, *J. Alloy Compd.* **2017**, *697*, 262.

[15] a) Y. Gao, M. D. Craven, J. S. Speck, S. P. DenBaars, E. L. Hu, *Appl. Phys. Lett.* **2004**, *84*, 3322; b) D. Li, M. Sumiya, S. Fuke, D. Yang, D. Que, Y. Suzuki, Y. Fukuda, *J. Appl. Phys.* **2001**, *90*, 4219.

[16] a) F. Liu, R. Collazo, S. Mita, Z. Sitar, G. Duscher, S. J. Pennycook, *Appl. Phys. Lett.* **2007**, 91; b) J. Zúñiga-Pérez, V. Consonni, L. Lymperakis, X. Kong, A. Trampert, S. Fernández-Garrido, O. Brandt, H. Renevier, S. Keller, K. Hestroffer, M. R. Wagner, J. S. Reparaz, F. Akyol, S. Rajan, S. Rennesson, T. Palacios, G. Feuillet, *Appl. Phys. Rev.* **2016**, 3; c) S. Keller, N. Fichrenbaum, F. Wu, G. Lee, S. P. DenBaars, J. S. Speck, U. K. Mishra, *Jpn. J. Appl. Phys.* **2006**, *45*, L322.

[17] J. Lemettinen, H. Okumura, I. Kim, M. Rudzinski, J. Grzonka, T. Palacios, S. Suihkonen, *J. Cryst. Growth* **2018**, *487*, 50.

[18] Z. Dou, Z. Chen, N. Li, S. Yang, Z. Yu, Y. Sun, Y. Li, B. Liu, Q. Luo, T. Ma, L. Liao, Z. Liu, P. Gao, *Nat. Commun.* **2019**, *10*, 5013.

[19] a) J. E. Northrup, J. Neugebauer, L. T. Romano, *Phys. Rev. Lett.* **1996**, *77*, 103; b) F. Liu, R. Collazo, S. Mita, Z. Sitar, S. J. Pennycook, G. Duscher, *Adv. Mater.* **2008**, *20*, 2162.

[20] a) N. Stolyarchuk, T. Markurt, A. Courville, K. March, O. Tottereau, P. Vennéguès, M. Albrecht, *J. Appl. Phys.* **2017**, *122*, 155303; b) N. Stolyarchuk, T. Markurt, A. Courville, K. March, J. Zuniga-Perez, P. Vennegues, M. Albrecht, *Sci. Rep.* **2018**, *8*, 14111.

[21] B. Jogai, *Phys. Rev. B* **1998**, *57*, 2382.

[22] a) H. K. Liu, Y. Wang, B. B. Zhang, Z. H. Yang, S. L. Pan, *Chem. Sci.* **2020**, *11*, 694; b) D. Holec, R. Rachbauer, D. Kiener, P. D. Cherns, P. M. F. J. Costa, C. McAleese, P. H. Mayrhofer, C. J. Humphreys, *Phys. Rev. B* **2011**, *83*, 165122.

[23] S. Ciraci, I. P. Batra, *Phys. Rev. B* **1983**, *28*, 982.

[24] a) J. E. Northrup, J. Neugebauer, *Appl. Phys. Lett.* **2004**, *85*, 3429; b) J. Song, G. Yuan, K. Xiong, B. Leung, J. Han, *Cryst. Growth Des.* **2014**, *14*, 2510.

[25] O. Ambacher, J. Smart, J. R. Shealy, N. G. Weimann, K. Chu, M. Murphy, W. J. Schaff, L. F. Eastman, R. Dimitrov, L. Wittmer, M. Stutzmann, W. Rieger, J. Hilsenbeck, *J. Appl. Phys.* **1999**, *85*, 3222.

[26] Z. Wan, A. Kazakov, M. J. Manfra, L. N. Pfeiffer, K. W. West, L. P. Rokhinson, *Nat. Commun.* **2015**, *6*, 7426.

[27] a) J. W. P. Hsu, M. J. Manfra, R. J. Molnar, B. Heying, J. S. Speck, *Appl. Phys. Lett.* **2002**, *81*, 79; b) B. Kim, D. Moon, K. Joo, S. Oh, Y. K. Lee, Y. Park, Y. Nanishi, E. Yoon, *Appl. Phys. Lett.* **2014**, 104.

[28] F. Dwikusuma, T. F. Kuech, *J. Appl. Phys.* **2003**, *94*, 5656.

[29] C. T. Nelson, B. Winchester, Y. Zhang, S.-J. Kim, A. Melville, C. Adamo, C. M. Folkman, S.-H. Baek, C.-B. Eom, D. G. Schlom, L.-Q. Chen, X. Pan, *Nano Lett.* **2011**, *11*, 828.